Bandi *et al. Molecular Cancer* (2025) 24:76
https://doi.org/10.1186/s12943-025-02288-9

Molecular Cancer

RESEARCH Open Access

ADT-1004: a first-in-class, oral pan-RAS inhibitor with robust antitumor activity in preclinical models of pancreatic ductal adenocarcinoma

Dhana Sekhar Reddy Bandi[1], Ganji Purnachandra Nagaraju[1], Sujith Sarvesh[1], Julienne L. Carstens[1], Jeremy B. Foote[2], Emily C. Graff[3], Yu-Hua D Fang[4], Adam B. Keeton[5,12], Xi Chen[5,12], Jacob Valiyaveettil[5,12], Kristy L. Berry[5], Sejong Bae[6], Mehmet Akce[1], Greg Gorman[7], Karina J. Yoon[8,13], Upender Manne[9], Michael R. Boyd[12], Donald J. Buchsbaum[10], Asfar S. Azmi[11], Yulia Y. Maxuitenko[5], Gary A. Piazza[5,12] and Bassel F. El-Rayes[1*]

Abstract

Background Oncogenic KRAS mutations occur in nearly, 90% of patients with pancreatic ductal adenocarcinoma (PDAC). Targeting KRAS has been complicated by mutational heterogeneity and rapid resistance. We developed a novel pan-RAS inhibitor, ADT-1004 (an oral prodrug of ADT-007) and evaluated antitumor activity in murine and human PDAC models.

Methodology Murine PDAC cells with $KRAS^{G12D}$ mutation (KPC-luc or 2838c3-luc) were orthotopically implanted into the pancreas of C57BL/6J mice, and four PDX PDAC tumors with KRAS mutations were implanted subcutaneously in NSG mice. To assess potential to overcome RAS inhibitor resistance, parental and resistant MIA PaCa-2 PDAC cells ($KRAS^{G12C}$ mutation) were implanted subcutaneously. Subcutaneously implanted RAS^{WT} BxPC-3 cells were used to assess the selectivity of ADT-1004.

Results ADT-1004 potently blocked tumor growth and RAS activation in mouse PDAC models without discernable toxicity with target engagement and reduced activated RAS and ERK phosphorylation. In addition, ADT-1004 suppressed tumor growth in PDX PDAC models with $KRAS^{G12D}$, $KRAS^{G12V}$, $KRAS^{G12C}$, or $KRAS^{G13Q}$ mutations and increased $CD4^+$ and $CD8^+$ T cells in the TME consistent with exhaustion and increased $MHCII^+$ M1 macrophage and dendritic cells. ADT-1004 demonstrated superior efficacy over sotorasib and adagrasib in tumor models resistant to these $KRAS^{G12C}$ inhibitors and MRTX1133 resistant $KRAS^{G12D}$ mutant cells. As evidence of selectivity for tumors with mutant KRAS, ADT-1004 did not impact the growth of tumors from RAS^{WT} PDAC cells.

Conclusion/Significance ADT-1004 has strong antitumor activity in aggressive and clinically relevant PDAC models with unique selectivity to block RAS-mediated signaling in RAS mutant cells. As a pan-RAS inhibitor, ADT-1004 has

*Correspondence:
Bassel F. El-Rayes
belrayes@uabmc.edu

Full list of author information is available at the end of the article

broad activity and potential efficacy advantages over allele-specific KRAS inhibitors. These findings support clinical trials of ADT-1004 for KRAS mutant PDAC.

Keywords Pancreatic ductal adenocarcinoma, pan-RAS inhibitor, Tumor immune microenvironment, KRAS, RAS-driven malignancies

Introduction

Pancreatic ductal adenocarcinoma (PDAC) is projected to become the second leading cause of cancer deaths in the US by 2040 [1, 2]. In 2024, PDAC is expected to cause 52,580 deaths in the US [3]. Systemic treatment strategies for PDAC have yielded little improvement in survival [4]. The overall survival rate at 5-years remains at 12% for patients diagnosed at early stages or 3% for those diagnosed with metastatic disease [5]. Hence, developing novel systemic treatment strategies is essential for improving the survival of patients with PDAC.

The gene encoding for KRAS, a small GTPase protein, is mutated in more than 90% of PDAC patients. KRAS mutations in patients with PDAC include G12D (37.0%), G12V (28.2%), G12R (12.7%), G12C (2.7%), or others (7.0%), and some have multiple mutations in RAS (2.1%) [6, 7]. The National Cancer Institute has identified anti-KRAS testing as one of four essential components for PDAC drug screening and development [8, 9]. Targeting this oncoprotein has proven challenging because it lacks a relatively flat surface for suitable small molecule binding sites [10]. To date, the U.S. Food and Drug Administration (FDA) has approved two $KRAS^{G12C}$ inhibitors, sotorasib (AMG-510) and adagrasib (MRTX849) for treatment of lung cancer. Several newer inhibitors targeting different KRAS mutations are in preclinical development or clinical trials. Sotorasib and adagrasib have limited use in PDAC, given that $KRAS^{G12C}$ is mutated in less than 3% of patients diagnosed with PDAC [11]. The development of adaptive resistance also limits the efficacy $KRAS^{G12C}$ inhibitors in patients diagnosed with $KRAS^{G12C}$ mutant cancers [12]. Resistance mechanisms include new KRAS mutations or activation of RAS^{WT} isozymes (HRAS and NRAS) from upstream receptor tyrosine kinases [13]. Consequently, a pan-RAS inhibitor could provide a broader and more effective approach to address the complex mutational landscape of PDAC that can escape compensatory mechanisms contributing to adaptive resistance.

To address the limitations of mutant-specific KRAS inhibitors, we developed and recently characterized ADT-007, a highly potent and selective pan-RAS inhibitor with broad activity against a histologically diverse range of RAS-mutant cancer cell lines. ADT-007 binds RAS in a nucleotide free conformation blocking GTP activation and disrupting downstream signaling through MAPK and AKT [14]. These effects result in ADT-007 inducing apoptosis by cleaved caspase 3 activation and cell cycle arrest at G2/M phase [14]. ADT-1004 is an orally bioavailable prodrug of ADT-007 designed to improve the water solubility and metabolic stability of ADT-007 (Fig. 1A). This study evaluated the antitumor activity and target selectivity of ADT-1004 in aggressive and clinically relevant mouse and PDX models of PDAC. We also defined various pharmacological attributes of ADT-1004 that could set this drug candidate apart from other KRAS inhibitors approved or in development.

Results

ADT-1004 inhibits tumor growth in murine models of PDAC

Initial experiments were conducted to confirm oral bioavailability and sufficient conversion of the prodrug, ADT-1004, to its active metabolite, ADT-007 *in vivo.* Following administration of a single oral dose of 100 mg/kg, ADT-1004 generated sustained plasma levels of ADT-007 for at least 8 h that were appreciably higher than growth IC_{50} values (Fig. 1B). Next, the maximum tolerated dose (MTD) of ADT-1004 was established. Dose-limiting toxicity was defined as weight loss of more than 10% of body weight or animal death. C57BL/6J mice implanted with subcutaneous tumors (SQ) were used in this experiment. ADT-1004 was administered by oral gavage BID, 5x/week for 3.5 weeks. The results revealed no significant differences in body weight between the vehicle and ADT-1004 treated groups at dosages up to 175 mg/kg BID. Significant weight loss was observed at doses of 200 mg/kg BID and higher (Fig. 1C). Blinded analysis of H&E-stained tissues from mice bearing SQ tumors treated with 175 mg/kg BID of ADT-1004 confirmed no discernable histopathologic abnormalities in the heart, lungs, kidneys, liver, jejunum, pancreas, and colon (Fig. 1D). In addition, analysis of clinical chemistries, complete blood counts, and bone marrow cytology revealed no significant differences in markers of liver and renal function, electrolytes, energy metabolism, and hematologic function in mice bearing SQ tumors treated with vehicle or ADT-1004 at the 175 mg/kg BID dose (Supplementary Fig. 1).

To determine the antitumor activity of ADT-1004, luciferase-labeled KPC (KPC-luc) cells with point mutations in $KRAS^{G12D}$ and $p53^{R172H}$ were surgically implanted into the pancreas of C57BL/6J mice. Mice were imaged one week after implantation (day 0) to randomize mice between the control (vehicle) and ADT-1004 treatment groups. Treatment was started on day 0 by once daily oral gavage with either vehicle or ADT-1004 at dosages ranging from 10 to 50 mg/kg (5x/week)

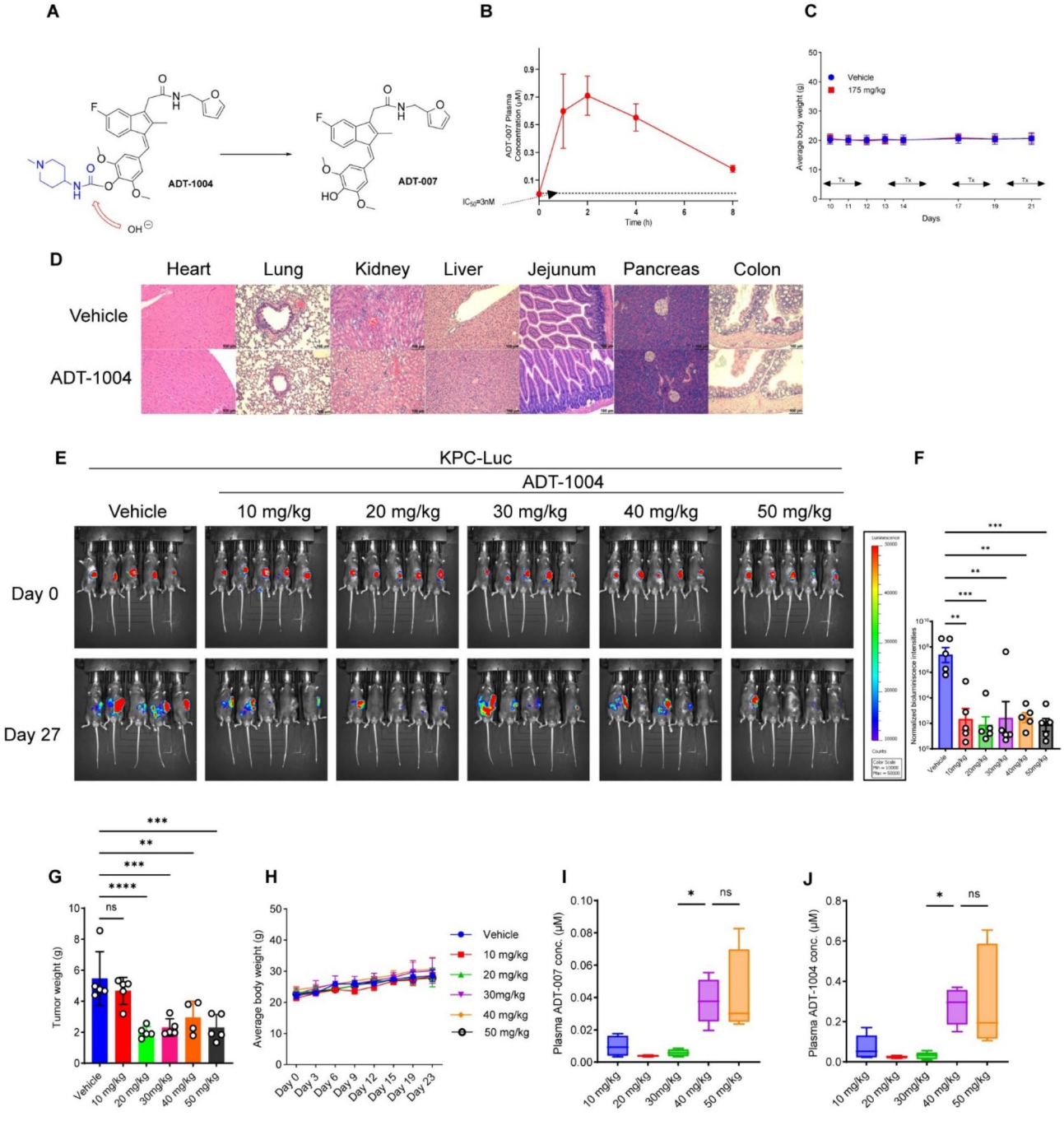

Fig. 1 Evaluation of ADT-1004 efficacy and toxicity profile in murine model of pancreatic cancer. (**A**). Chemical structures of ADT-1004 and ADT-007. (**B**). Plasma levels of ADT-007 in mice following a single oral administration of ADT-1004 (100 mg/kg, mean ± SD, $n = 3$–4). Dash line shows ADT-007 IC_{50} (3 nM) for MIA PaCa-2 PDAC cells in vitro. (**C**). Body weights of C57BL/6J mice treated with ADT-1004 (175 mg/kg, $n = 5$) or vehicle ($n = 10$) orally BID, 5x/week for 3.5 weeks. (**D**). Histopathological examination of vital organs (heart, lung, kidney, liver, jejunum, pancreas, and colon) from mice treated with ADT-1004 at 175 mg/kg BID as assessed by H&E staining. (**E**). *F*-Luc-labeled KPC cells were orthotopically implanted into C57BL/6J mice ($n = 30$). After 1 week, groups of 5 mice were orally administered vehicle or ADT-1004 (10, 20, 30, 40, and 50 mg/kg). Bioluminescence images at the indicated time points are shown. (**F**). Relative normalized whole-body bioluminescence intensities in mice under the indicated conditions ($n = 5$) (**G**). Tumors weights at the indicated conditions for experiment in (**E**). Note that one of the animals in 40 mg/kg group died on day 27 of the study prior to necropsy and thus excluded from the analysis. (**H**). Average body weights of the animals during the treatment shown in experiment (**E**). (**I**). The concentration of ADT-007 in plasma of mice on the last day of treatment ($IC_{50} < 6$ nM for KPC cells). (**J**). The concentration of ADT-1004 in plasma of mice on the last day of treatment. All quantitative data represent the mean ± SEM. ANOVA was used as statistical test. ns, non-significant, $*p < 0.05$, $**p < 0.01$, $***p < 0.001$, and $****p < 0.0001$

(Fig. 1E). Mice were euthanized on day 27 to determine treatment effects on tumor growth by measuring bioluminescence and tumor weight (Fig. 1F and G). Most mice in the ADT-1004 treatment groups displayed reduced bioluminescence compared with mice treated with vehicle. Doses of ADT-1004 from 20 to 50 mg/kg demonstrated comparable statistically significant reductions in tumor weights compared to vehicle-treated mice or mice treated with 10 mg/kg ADT-1004 (Fig. 1G). There were no significant differences in body weight between the ADT-1004 treated and vehicle groups (Fig. 1H).

Measurement of ADT-1004 and ADT-007 levels in plasma by LC-MS/MS was performed 6 h after administration of the last dose. Peak concentration in plasma for ADT-007 occurred at 2 h post dose administration (Fig. 1C). Observed average plasma concentrations of ADT-007 from animals treated with 20, 30, 40, and 50 mg/kg were 3.4, 5.7, 31.2 and 54.1 nM, respectively (Fig. 1I) and these are within the IC_{50} range. The 40 mg/kg dose generated comparable plasma levels to the 50 mg/kg dose (Fig. 1I and J) both of which were significantly higher compared to plasma levels generated by the 10, 20, and 30 mg/kg doses. Hence we selected 40 mg/kg dose for further experiments.

Tumor growth inhibition by ADT-1004 is associated with reduced activated RAS and pERK levels

The mechanism responsible for the anti-cancer activity of ADT-007 was previously reported to involve direct binding to RAS within the nucleotide-binding domain to block GTP activation of RAS and suppress effector interactions and downstream MAPK/AKT signaling [14]. We, therefore, conducted a second experiment using the KPC orthotopic model described above to confirm that ADT-1004 inhibits tumor growth by blocking RAS activation. Similar to results from the first experiment, oral administration of ADT-1004 at a dosage of 40 mg/kg demonstrated a significant reduction in tumor growth compared with the vehicle group, as evidenced by the bioluminescence imaging and tumor weight without differences in body weight (Fig. 2A-E). The tumor tissues were analyzed for immune changes using multi-parameter flow cytometry to identify myeloid, T, NK, and tumor cells in the TME (Fig. 2F). Consistent with in vitro studies of ADT-007 [14], measurement of activated RAS levels by RAS-RBD pull-down assays showed that tumors from ADT-1004 treated mice had significantly reduced RAS-GTP levels compared with tumors from vehicle-treated mice (Fig. 2G). Tumors from mice in the treated with ADT-1004 also showed reduced pERK levels (~60%) compared with the vehicle group (Fig. 2H).

Next, we determined the antitumor activity of ADT-1004 in additional mouse PDAC models. Given the plasma concentration of ADT-007 observed at 6 h after administration of the 20 mg/kg dose was within the lower range of IC_{50}, we determined whether a twice daily schedule could improve the therapeutic efficacy by maintaining steady therapeutic plasma drug levels and potentially improve antitumor activity compared to once daily dosing. We employed a different syngeneic, immunocompetent orthotopic mouse model in which 2838c3-luc cells were implanted into the pancreas of female C57BL/6J mice (Fig. 3A). Mice were treated 5x/week with either vehicle or ADT-1004 at 20 mg/kg QD, 20 mg/kg BID, or 40 mg/kg QD. Measurement of bioluminescence and tumor weights showed that ADT-1004 comparably reduced tumor growth with no significant differences in body weight compared with the vehicle group (Fig. 3A-E). As we did not observe any additional anti-tumor activity for the BID dosing and decided not to pursue further.

We also determined if the antitumor activity of ADT-1004 in the 2838c3 orthotopic PDAC model was associated with reduced levels of activated RAS. Similar to results in the KPC orthotopic model, RAS-RBD pull-down assays showed a significant reduction (~70%) of RAS-GTP levels in tumors from ADT-1004-treated mice compared with tumors from vehicle-treated mice (Fig. 3F). A notable decrease, albeit less dramatic than seen in KPC, in the pERK levels was also observed in mice treated with ADT-1004 at the 40 mg/kg dose (~60%), providing additional evidence that the antitumor activity of ADT-1004 is mediated by inhibition of activated RAS (Fig. 3G) and consistent with previous in vitro studies of ADT-007 [14].

ADT-1004 alters tumor immune microenvironment (TiME) by inhibiting KRASG12D

Considering the growing literature reporting that mutation-specific KRAS inhibitors can enhance tumor-specific immunity [15, 16], we investigated the activity of ADT-1004 in two PDAC-bearing, syngeneic, immunocompetent mouse models harboring the $KRAS^{G12D}$ mutation (KPC and 2838c3). Both cell lines expressed $KRAS^{G12D}$ and exhibited increased T cell infiltration with an effector phenotype [14]. In the 2838c3 model, the effector phenotype of $CD8^+$ T cells which have high levels of PD-1 and CTLA-4 expression were previously demonstrated to be responsive to combinatorial immune checkpoint blockade (ICB) utilizing antagonists to PD-1 and CTLA-4 [17]. Given our previous findings involving direct injection of ADT-007 in subcutaneous syngeneic mouse PDAC models, including 2838c3 [14], we assessed the numbers and phenotype of T, NK, and myeloid cell subsets by multiparameter flow cytometry to determine whether ADT-1004, as a prodrug of ADT-007, had a similar impact on immune subset abundances and phenotypes in the pancreatic TME.

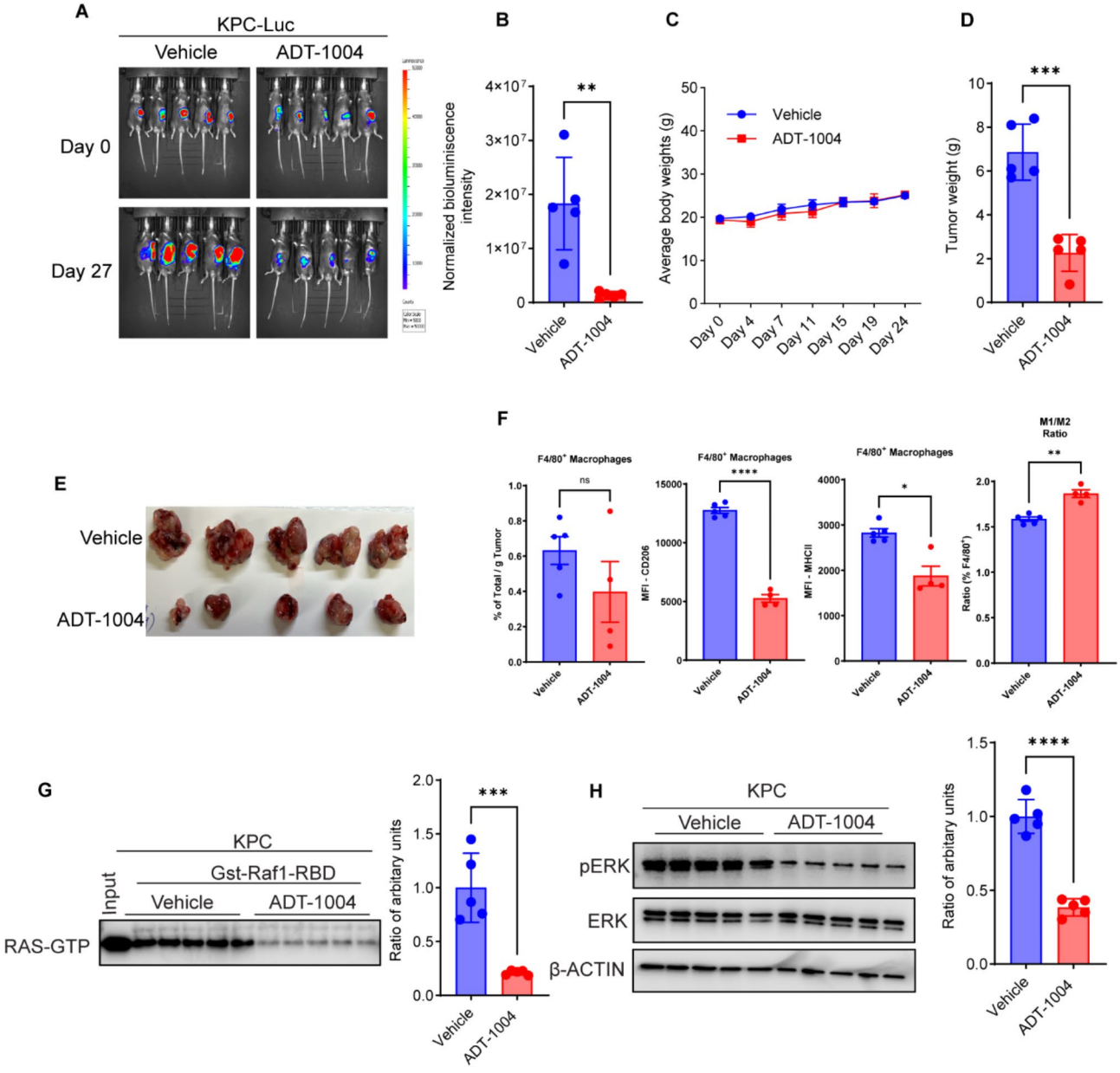

Fig. 2 Effect of ADT-1004 treatment on tumor growth and molecular markers in KPC cell-implanted C57BL/6J mice. (**A**). KPC-luc cells were injected orthotopically into the pancreas of C57BL/6J mice. Representative bioluminescence images at the indicated time points are shown. (**B**). Relative normalized whole-body bioluminescence intensities in mice under the indicated conditions ($n=5$). (**C**). Average body weights of mice treated with vehicle and ADT-1004 (40 mg/kg). (**D**). Tumor weights were measured from mice at the end of the experiment under the indicated conditions for experiment in (**A**). (**E**). Tumor images at the end of the experiment are shown. (**F**) The percentages of $CD45^+$ $CD11b^+$ F4/80, and $CD206^+$ (macrophages), $CD11b^+$ $F4/80^+$ PD-$L1^+$, and M1/M2 ratios increased in tumors from ADT-1004 treated ($n=4$) compared to vehicle ($n=5$) treated mice. (**G**). The tumors were probed for detecting activated RAS GTP levels by GST-Raf1-RBD pull-down assay (left) and graph depicting quantification of activated RAS GTP levels (right). (**H**). Indicated tumor tissues were analyzed for pERK and total ERK by immunoblotting. β-Actin was used as a loading control (left). Graph depicting quantification of pERK normalized using β-Actin (right). All quantitative data represent the mean ± SEM. t-test was used for statistical analysis. ns, non-significant, $*p<0.05$, $**p<0.01$, $***p<0.001$, and $****p<0.0001$

Following 28 days of treatment course (5x/week), mice bearing KPC or 2838c3 tumors were euthanized to evaluate changes in the immune cell population densities within the pancreatic TME. ADT-1004 treatment increased the density (% Total/gm tumor) of innate-like (TNK and γδT) or NK cells in the 2838c3 and KPC models (Supplementary Fig. 2A and 2B) in agreement with previous ADT-007 findings [14]. Furthermore, ADT-1004 treatment increased the density of $CD4^+$ and $CD8^+$ T cells in the 2838c3 TME (Fig. 3H-I) despite remaining

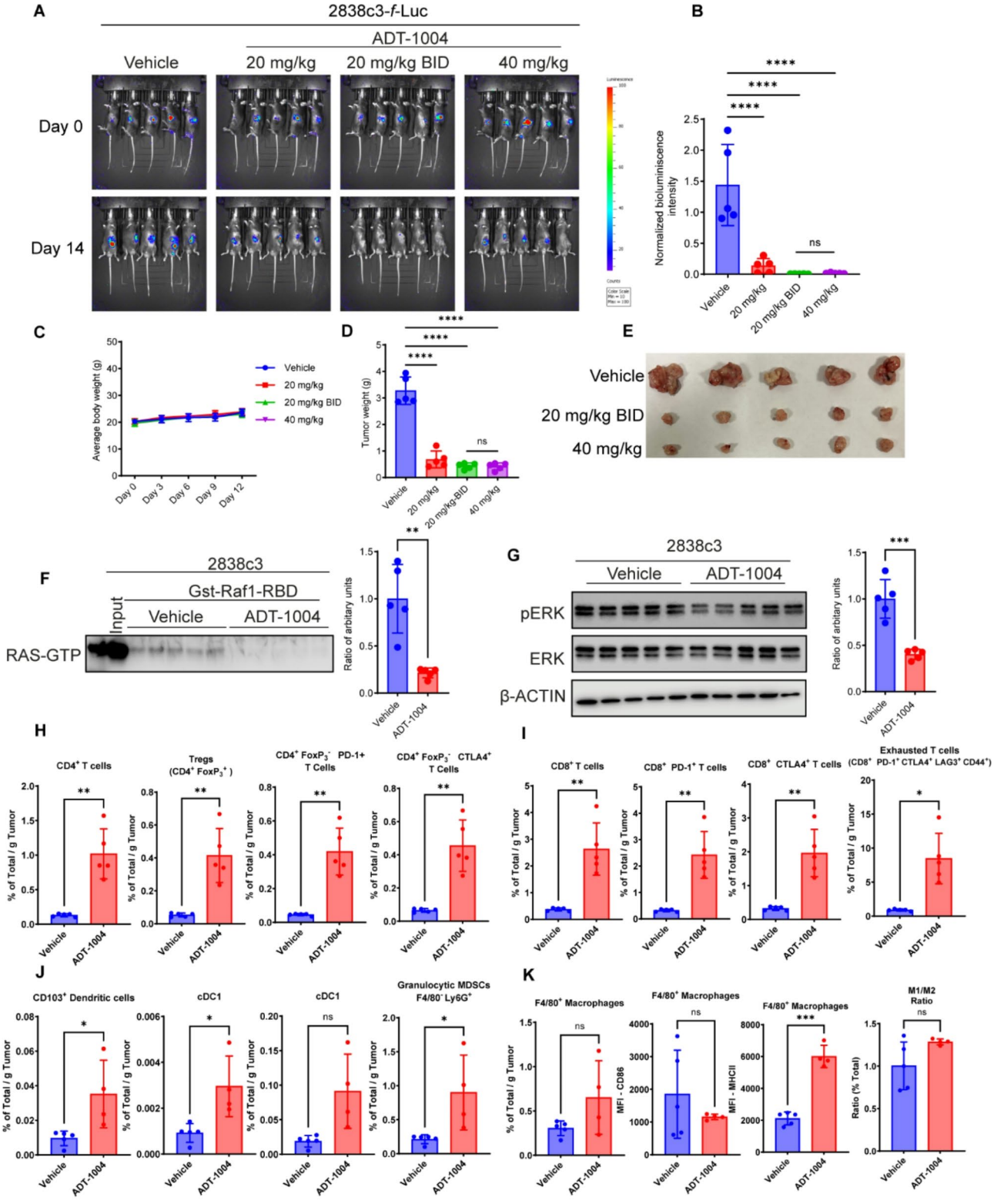

Fig. 3 (See legend on next page.)

(See figure on previous page.)

Fig. 3 ADT-1004 treatment suppresses tumor growth and modulates tumor microenvironment in C57BL/6J mice with 2838c3 cell implants. (**A**). F-Luc-labeled 2838c3 cells were orthotopically implanted into C57BL/6J mice ($n=20$). Four groups of 5 mice were treated with vehicle or ADT-1004 by oral gavage (20 mg/kg, 20 mg/kg BID, and 40 mg/kg body weight) 5 days/week per week. (**B**). Normalized bioluminescence intensities of the tumors in the 4 groups of mice. (**C**). Average body weights of the animals during the treatment shown in experiment (**A**). (**D**). Tumor weights were measured from mice at the end of the experiment for indicated dosing schedules (**A**). (**E**). Tumor images at the end of the experiment are shown for vehicle and ADT-1004 (20 mg/kg BID and 40 mg/kg). (**F**). Indicated tumor tissues were probed for detecting activated RAS GTP levels by GST-Raf1-RBD pull-down assay (left). Graph depicting the quantification of activated RAS GTP levels (right). (**G**). Indicated tumor tissues were analyzed for pERK and total ERK. β-Actin was used as a loading control (left). Graph depicting the quantification of pERK normalized using β-Actin (right). (**H**). Proportions of $CD4^+$ T-cells, $CD4^+$ $Foxp3^+$, $CD4^+$ $PD\text{-}1^+$ T cells, and $CD4^+$ $CTLA\text{-}4^+$ T cells in 2838c3 TiME in ADT-1004 ($n=5$) and vehicle ($n=5$) treated mice. (**I**). Expression of $CD8^+$ T-cells, $CD8^+$ $PD\text{-}1^+$ T cells, $CD8^+$ $PD\text{-}1^+$ $LAG3^+$, and $CD8^+$ $PD\text{-}1^+$ $CTLA\text{-}4^+$ subsets from 2838c3 TME. (**J**). The percentages of $CD11b^+$ $MHCII^{hi}$, $XCR1^+$ cDC1, and $CD11b^+$ $CD11c^{hi}$ $MHCII^{hi}$ $CD172\alpha^+$ cDC2 subsets increased in ADT-1004 ($n=5$) compared to vehicle ($n=5$) treated mice. (**K**). The percentages of $CD45^+$ $CD11b^+$ F4/80, and $CD206^+$, $CD11b^+$ $F4/80^+$ $PD\text{-}L1^+$, M1/M2 ratio increased in ADT-1004 treated ($n=5$) compared to vehicle ($n=5$) treated mice. ANOVA and Welch's t-test was used for statistical analysis where appropriate. Error bars indicate SD. ns, non-significant, $*p<0.05$, $**p<0.01$, $***p<0.001$, and $****p<0.0001$

unchanged in the KPC TME (Supplementary Fig. 3A-B). Phenotypic analysis revealed that ADT-1004 treatment caused a marked increase in the density of $CD4^+$ and $CD8^+$ $PD\text{-}1^+$ and $CD4^+$ $CTLA4^+$. (Fig. 3H-I). However, no significant difference was identified in KPC tumors treated with ADT-1004 (Supplementary Fig. 3B). Furthermore, the densities of $CD4^+$ and $CD8^+$ T cells co-expressing PD-1, CTLA4, LAG-3, and CD44 (Fig. 3I) were increased in 2838c3 tumors after ADT-1004 treatment, indicating an emergence in exhaustion phenotype in the 2838c3 model. Overall, these findings indicate an increase in the density of innate-like NKT, γδT, activated and potentially exhausted $CD4^+$ and $CD8^+$ T cells after ADT-1004 treatment in the 2838c3 model.

Analysis of myeloid cells after ADT-1004 treatment revealed an increased density (% total/mg tumor) of $F4/80^+$ macrophages, $XCR1^+$ cDC1, $CD172\alpha^+$ cDC2, and $Ly6G^+$ granulocytes in the 2838c3, but not KPC TME (Fig. 3J + K and Supplementary Fig. 3C), which has a higher density of $F4/80^+$ macrophage compared to 2838c3 (Fig. 2F). More importantly, in both models, $F4/80^+$ macrophages exhibited an increased ratio of M1-like ($MHCII^{hi}$) macrophages compared to M2 ($CD206^+$) like macrophages (Figs. 2F and 3K) suggesting potential within the TME improved anti-tumor immune responses, synergy of immune checkpoint receptor blockade of PD-1, CTLA4, and/or LAG-3 with ADT-1004. Additional work utilizing these combinations in each model is warranted.

Spatial phenotyping reveals enhancement of TME infiltration in ADT-1004 treated tumors

We next sought to investigate the effects of ADT-1004 on the cellular infiltration patterns within the tumor core. Since the 2838c3 model showed higher immune infiltration, we further selected this model for spatial phenotyping. Pancreatic tumors from the 2838c3-luc murine PDAC model were initially assessed for viable tumor cores by a licensed veterinary pathologist and 3 mm cores were obtained to generate a microarray of each tumor ($n=4$ for each treatment group). We performed multiplex immunofluorescence using the Lunaphore COMET system and a 15-plex antibody marker panel for general neoplastic, immune, and stromal cell profiling (Fig. 4A). Cells were classified into 13 distinct phenotypes based on marker positivity: cancer cells CK^{Bright}, cancer cells CK^{Dim}, B-cells ($CD19^+$), undefined T cells (T cells (other): $CD3^+CD8^-CD4^-$), cytotoxic T cells (CytoT: $CD3^+$ $CD8^+$), T effector cells (Teff: $CD3^+$ $CD4^+$), T regulatory cells (Treg: $CD3^+$ $CD4^+$ $Foxp3^+$), macrophages (Mac: $CD11b^+$ $Ly6G^-$), Neutrophils (Neutro: $CD11b^-$ $Ly6G^+$), myeloid derived suppressor cells (MDSC: $CD11b^+$ $Ly6G^+$), cancer-associated fibroblasts (CAF: any combination of FAP^+, αSMA^+, $PDGFR\beta^+$, $Desmin^+$, or $Integrin\beta3^+$), and undefined cells (negative for all markers).

Initially, count-based metrics showed no significant differences between the treatment groups in the proportion of neoplastic, stromal, or immune cell compartments (Fig. 4A). Within the neoplastic cellular compartments, there were also no differences in the proportions of cancer cell subtypes (Fig. 4B). When assessing mesenchymal marker co-expression, (Fig. 4C), an increase in epithelial markers was noted. The immune cell count showed a significant increase in T effector cells in the ADT-1004 treated, 2838c3 tumors matching the observations obtained from the dissociative immune phenotyping (Figs. 3H-K and 4D). Within the stromal compartment, there were no significant differences in the percentages of CAFs both in aggregate and in the single marker expression patterns (Fig. 4E). There was a trending increase in the number of endothelial and immune cell infiltrates in the ADT-1004 treated tumors (Fig. 4F) suggesting an increase in vascularization post-treatment.

To assess the effects of ADT-1004 treatment on the cellular infiltration patterns of the core TME, we performed the G-function analysis that quantifies the infiltration of one cell-type (neighbor) within specified radii of another cell type (target). We performed this analysis for sets of 10 μm radii ranging from cell-cell contact distances 10–50 μm through non-cell contact distances (60–200 μm). The significance between the vehicle and ADT-1004 groups was calculated for each pair-wise comparison at each radius. We observed both $Cancer^{CKbright}$ and $Cancer^{CKdim}$ cells had significantly more endothelial

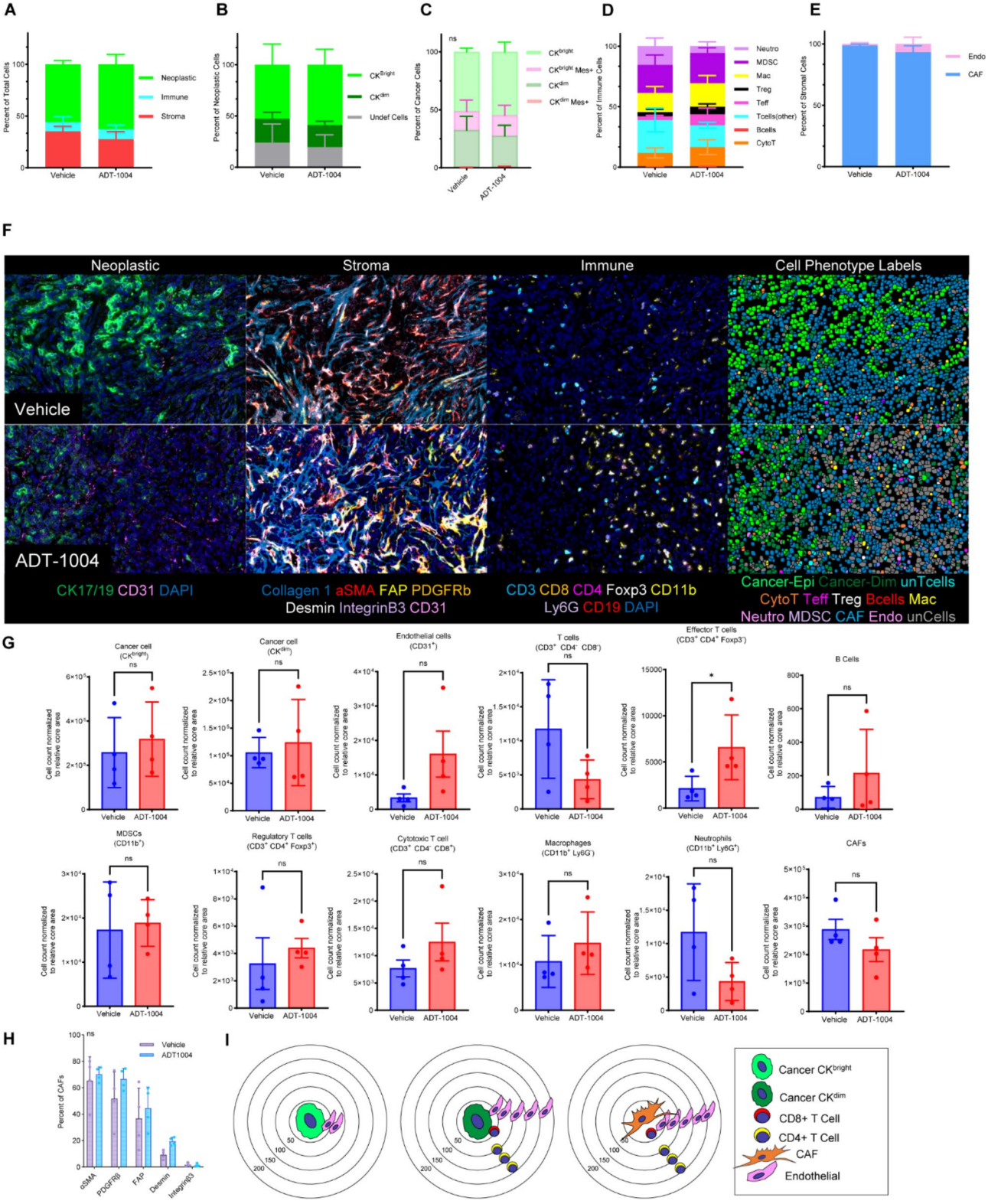

Fig. 4 (See legend on next page.)

(See figure on previous page.)

Fig. 4 Spatial quantification reveals increased immune infiltration in ADT-1004 treated TME. (**A**). The expression matrix for each of the cell phenotypes based on Visiopharm results. (**B**). Percentage of neoplastic cells (y-axis) in each tumor (color legend) for each core of the TMA (x-axis). (**C**). Mesenchymal expressing CK^{dim} cells in ADT-1004 treated tumors did not co-localize with CD8 + or CD4 + T cells. (**D**). Percentage of immune cells (y-axis) in each tumor (color legend) for each core of the TMA (x-axis). (**E**). Annotations of classified neoplastic and immune cells (top) in the vehicle (left) and ADT-1004 treatments (right) and the corresponding antigens detected in the multi-color fluorescence images (bottom). (**F**). The t-distributed stochastic neighbor embedding (tSNE) plot showed 13 clusters (color legend) in a single core (left). Expression programs of different cell phenotypes (right) in the vehicle and ADT-1004 treated cores. tSNEs of single-nucleus profiles (dots) of neoplastic cells (cancer-epi, cancer-dim, and CAFs) from all tumors, and immune compartments (Macrophages, cyto T cells, T cells, Teff, and Tregs). (**G**). Unchanged CK^{bright} and CK^{dim} cells and increasing trend in endothelial cell infiltration in ADT-1004 treated TMAs compared to vehicle. Unchanged Tregs, significantly increased Teff, increased Teff/Treg ratio, and increased B cells in ADT-1004 treated TMAs compared to vehicle. Increased monocytic MDSCs ($CD11b^+$ $Ly6G^-$) and decreased granulocytic MDSCs ($CD11b^+$ $Ly6G^+$) in ADT-1004 treated TMAs compared to vehicle. Slightly reduced CAFs and increased endothelial cells in ADT-1004 treated TMAs compared to vehicle. (**H**). Unchanged percentage of CAFS in (α-SMA, PDGFRβ, FAP, Desmin, and Integrinβ3). (**I**). Reduced pericytic coverage in ADT-1004 treated tumors compared to vehicle in endothelial cells (left). Mesenchymal expressing CK^{dim} cells in ADT-1004 treated tumors did not co-localize with $CD8^+$ or $CD4^+$ T cells (middle). FAP^+ and $Integrin\beta3^+$ CAFs exclude $CD8^+$ T cells
$Integrin\beta3^+$ CAFs exclude $CD4^+$ T cells (right). Welch's t-test was used for statistical analysis. ns: not significant and $*p < 0.05$

cell infiltration in the ADT-1004 treated tumors suggesting better vasculature coverage (Fig. 4F and G). In addition to this, we could not identify any significant difference in the proportions of CAF percentage in ADT-1004 treated tumors compared to tumors from the vehicle group (Fig. 4H). Both $Cancer^{CKdim}$ and CAF cells had increased $CD8^+$ cell infiltration within cell-cell contact radii and Teff infiltration within near secretory distances of 100–150 µm (Fig. 4I, Supplementary Fig. 4A-C), which correlate with known functions of cell-cell contact and cytokine secretion for these cell types [14].

We next determined if specific mesenchymal markers (αSMA, FAP, Desmin, PDGFRβ, or Integrinβ3) in the target cells were associated with immune cell infiltration patterns. $Cancer^{CKdim}$ cells that co-expressed any mesenchymal marker were not co-localized with the $CD8^+$ or $CD4^+$ cells. This observation confirmed previous spatial infiltration observations in mouse and human PDAC samples of reduced T cell infiltration around mesenchymal expressing cancer cells [18]. Analysis of mesenchymal marker expression in the target CAF population showed FAP^+ and $Integrin\beta3^+$ CAFs excluded $CD8^+$ T cells in the ADT-1004 treated tumors and $Integrin\beta3^+$ CAFs excluded $CD4^+$ cells; all other mesenchymal markers had no association with immune cell infiltration. Marker expression analysis of the neighbor cells showed that ADT-1004 treated tumors had a significant increase in infiltration of $CD11b^-$ $CD8^+$ and $CD4^+$ cells around $Cancer^{CKdim}$ and CAF cells. These data demonstrate the enhancement of immune cell infiltration with ADT-1004 treatment.

ADT-1004 inhibits the growth of KRAS mutant PDX tumors

Given previous reports that ADT-007 inhibits the growth of KRAS mutant cancer cells regardless of the KRAS mutation, we determined the antitumor activity of ADT-1004 across a panel of PDAC PDX models harboring three different KRAS mutations ($KRAS^{G12D}$, $KRAS^{G12C}$, and $KRAS^{G13Q}$) and one pancreaticobiliary PDX model ($KRAS^{G12V}$). Tumor fragments from each of the PDX models were subcutaneously implanted into the right flank of NSG mice. Body weight and tumor volumes were measured while the mice were treated orally with ADT-1004 once daily at a dose of 40 mg/kg (5x/week). Tumor weights were determined at the end of the experiment. ADT-1004 treatment significantly inhibited the growth of PDAC tumors with $KRAS^{G12D}$ (Fig. 5A and C, Supplementary Fig. 5A), $KRAS^{G12C}$ (Fig. 5E and G, Supplementary Fig. 5B), $KRAS^{G12V}$ (Fig. 5I and K, Supplementary Fig. 5C) and $KRAS^{G13Q}$ (Fig. 5M and O, Supplementary Fig. 5D) with no change in body weight over the course of treatment, further demonstrating tolerability at dosages that inhibit tumor growth (Fig. 5B, F and J, and 5N, respectively).

Immunohistochemical (IHC) analysis of the four KRAS mutant PDX tumor models revealed multiple effects of ADT-1004 treatment. We observed a significant reduction of pERK levels in tumors from mice treated with ADT-1004 compared to mice treated with vehicle. In addition, αSMA immunostaining resulted in decreased expression within the ADT-1004 treatment group with distinct changes indicating structural reorganization, tissue remodeling, or fibrotic processes. Finally, analysis of Ki-67 levels showed a marked decrease in proliferative activity in all four treatment groups relative to their respective vehicle group, G12D (Fig. 6A), G12C (Fig. 6B), G12V (Fig. 6C) and G13Q (Fig. 6D) mutant expressing tumors.

ADT-1004 does not inhibit tumor growth of RASWT PDAC cells

Additional experiments were performed to confirm the RAS selectivity of ADT-1004, given previous studies reporting that RAS^{WT} cancer cells with downstream BRAF mutations and cells from normal tissues were insensitive to ADT-007 [14]. Male NSG mice were implanted subcutaneously with BxPC-3 (RAS^{WT} $BRAF^{V600E}$) cells and treated with 40 mg/kg ADT-1004 for 31 days. Body weight and tumor volume were

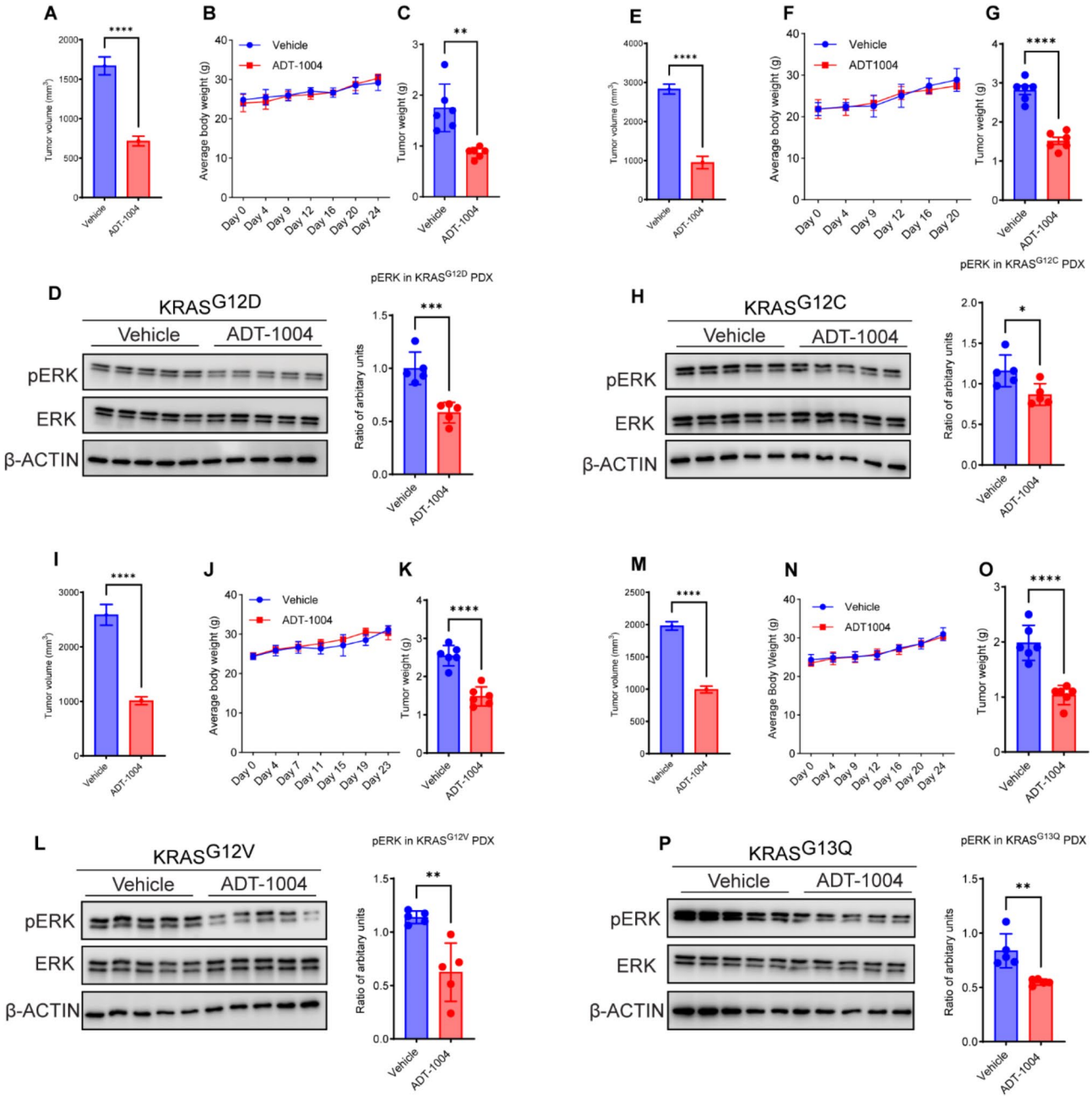

Fig. 5 ADT-1004 treatment suppresses tumor growth and downregulates pERK levels in KRAS-mutant PDX models. (**A**). Tumor growth curves of $KRAS^{G12D}$ PDX implanted subcutaneously into NSG mice and treated with vehicle or ADT-1004 ($n=6$). (**B**). Average body weights of mice treated with vehicle and ADT-1004 (40 mg/kg). (**C**). Tumor weights at the end of the experiment under the indicated conditions. (**D**). The indicated tumor tissues were probed for measuring pERK and total ERK. β-Actin was used as a loading control. Graph depicting the quantification of pERK by western blot analysis, normalized using β-Actin (left). (**E**) Tumor growth curves of $KRAS^{G12C}$ PDX implanted subcutaneously into NSG mice ($n=6$). (**F**). Average body weights of mice treated with vehicle and ADT-1004 (40 mg/kg). (**G**). Tumor weights were measured from mice at the end of the experiment. (**H**). The indicated tumor tissues were probed for measuring pERK and total ERK. β-Actin was used as loading control (right). Graph depicting the quantification of pERK by western blot analysis, normalized using β-Actin (left). (**I**). Tumor growth curves of $KRAS^{G12V}$ PDX implanted subcutaneously into NSG mice ($n=6$). (**J**). Average body weights of the animals during the treatment. (**K**). Tumor weights from mice at the end of the experiment. (**L**). The indicated tumor tissues were probed for measuring pERK and total ERK. β-Actin was used as loading control (right). Graph depicting the quantification of pERK by western blot analysis, normalized using β-Actin (left). (**M**) Tumor growth curves of $KRAS^{G13Q}$ PDX implanted subcutaneously into NSG mice ($n=6$). (**N**). The average body weights of the animals during the treatment. (**O**) Tumor weights at the end of the experiment under the indicated conditions. (**P**) The indicated tumor tissues were probed for measuring pERK and total ERK. β-Actin was used as loading control (right). Graph depicting the quantification of pERK by western blot analysis, normalized using β-Actin (left). Data represent the mean ± SEM. Welch's t-test was used for statistical analysis. $^{*}p<0.05$, $^{**}p<0.01$, $^{***}p<0.001$, and $^{****}p<0.0001$

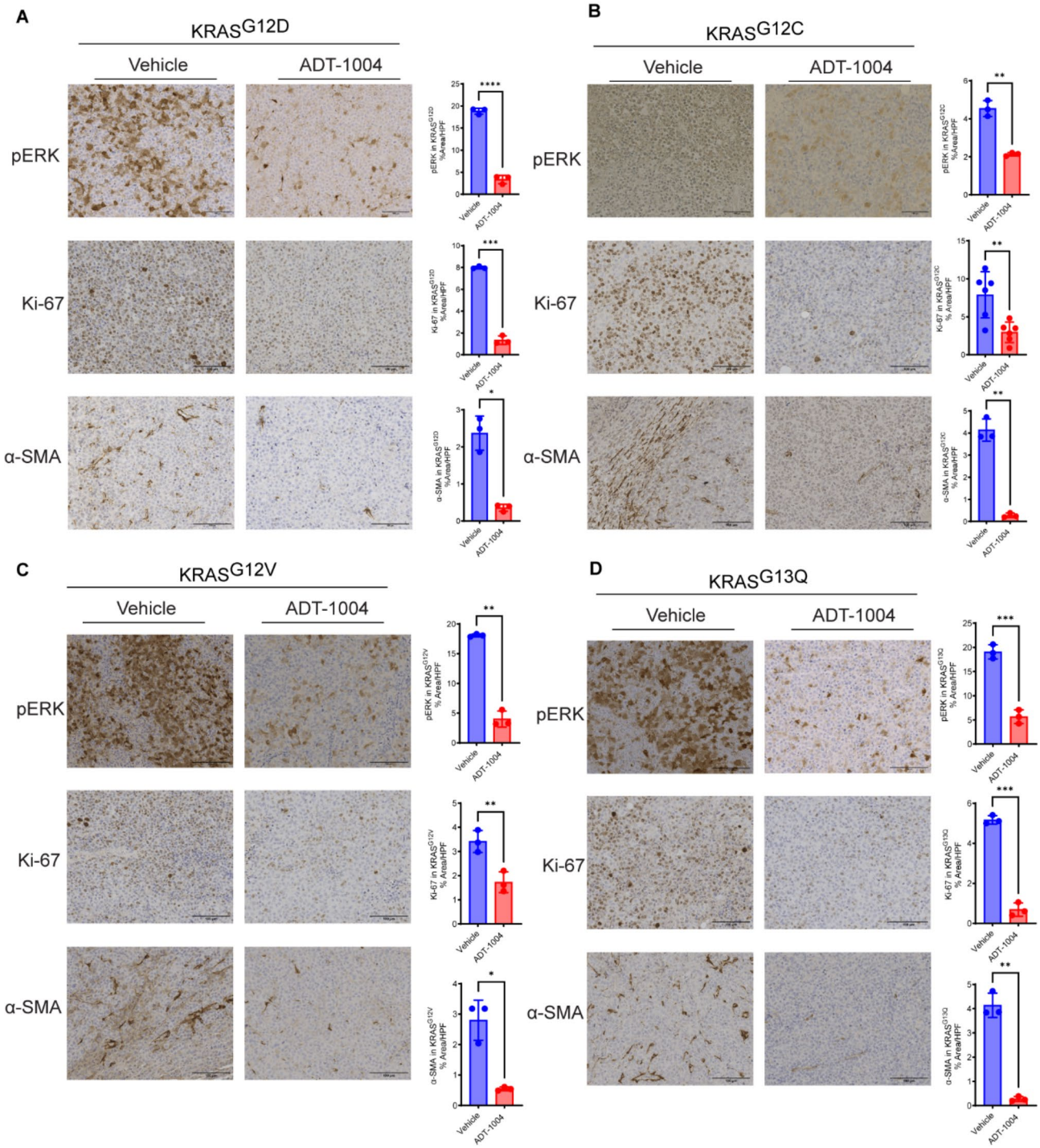

Fig. 6 ADT-1004 treatment downregulates molecular markers in KRAS-mutant PDX models. (**A**). Representative IHC images of pERK, αSMA, and Ki-67 (left) and quantifications of IHC results (right) in $KRAS^{G12D}$ PDX model. (**B**). Representative IHC images of pERK, αSMA, and Ki-67 (left) and quantifications of IHC results (right) in $KRAS^{G12C}$ PDX model. (**C**). Representative IHC images of pERK, αSMA, and Ki-67 (left) and quantifications of IHC results (right) in $KRAS^{G12V}$ PDX model. (**D**). Representative IHC images of pERK, αSMA, and Ki-67 (left) and quantifications of IHC results (right) in $KRAS^{G13Q}$ PDX model. Data represent the mean ± SEM. Welch's t-test was used for statistical analysis. *$p < 0.05$, **$p < 0.01$, ***$p < 0.001$, and ****$p < 0.0001$

monitored twice weekly throughout the study. ADT-1004 treatment did not significantly affect BxPC-3 tumor growth (Supplementary Fig. 6A) or impacted body weight (Supplementary Fig. 6B), with no statistically significant difference observed in tumor weights (Supplementary Fig. 6 C-6D). These results lead us to conclude that ADT-1004 selectively inhibits RAS-dependent tumor growth in mouse tumor PDAC models and are consistent with

previous reports characterizing the in vitro growth inhibitory activity of ADT-1004 [14].

ADT-1004 inhibits tumor growth of PDAC cells resistant to KRASG12C and KRASG12D inhibitors

Human MIA PaCa-2 $KRAS^{G12C}$ cells resistance to sotorasib and adagrasib was confirmed by in vitro experiments to determine growth IC_{50} values against the parental MIA PaCa-2 cells [19]. MIA PaCa-2 $KRAS^{G12C}$ cells showed remarkable sensitivity to ADT-007 with an IC_{50} value of 3 nM, while sotorasib and adagrasib were less potent with IC_{50} values of 28 and 21 nM, respectively (Fig. 7A). MIA PaCa-2 cells that developed resistance to sotorasib and adagrasib (MIA-AMG-R) cells were only slightly less sensitive to ADT-007 with an IC_{50} value of 16 nM, but completely lost sensitivity to sotorasib and adagrasib (Fig. 7B). Similarly, AsPC-1 $KRAS^{G12D}$ cells resistant to MRTX1133 [20] retained sensitivity to ADT-007 (Supplementary Fig. 7). In addition, ADT-007, sotorasib, and adagrasib inhibited colony formation in parental MIA PaCa2 cells. However, the differences in potency and extent of killing caused by ADT-007 compared with sotorasib and adagrasib were more pronounced, which may reflect the ability of ADT-007 to induce mitotic arrest and apoptosis as previously reported [14]. Similar to growth assays, ADT-007 retained activity to inhibit colony formation in MIA-AMG-R cells, while sensitivity to sotorasib and adagrasib was markedly diminished (Fig. 7C and D).

Next, experiments utilizing NSG mice xenografted subcutaneously with parental MIA PaCa-2 and MIA-AMG-R cells were conducted. Mice implanted with parental MIA PaCa-2 cells showed comparable decreased tumor volume (Fig. 7E) and final tumor weights (Fig. 7F and G), following treatment with ADT-1004, sotorasib or adagrasib, each at a once-daily dose of 40 mg/kg (5x/week). No significant differences in body weight were measured across treatment and vehicle groups (Supplementary Fig. 8A). In addition, we found a significant reduction in pERK levels in tumors in all the treatment groups compared to tumors from vehicle-treated mice (Fig. 7H and Supplementary Fig. 8C). In a side-by-side comparison, oral administration of ADT-1004 led to a dramatic decrease in tumor volume (Fig. 7I) and weight (Fig. 7J and K) compared with vehicle against tumors derived from MIA-AMG-R cells. By contrast, neither sotorasib nor adagrasib were effective. Notably, ADT-1004 demonstrated antitumor activity without any visible change in the body weights of treated mice (Supplementary Fig. 8B). Furthermore, western blotting for the detection of pERK showed a significant reduction in the ADT-1004 treated tumors compared to all other treatment or vehicle groups, while neither sotorasib or adagrasib impacted pERK levels (Fig. 7L and Supplementary Fig. 8D). These results show that ADT-1004 is highly effective against $KRAS^{G12C}$ tumors resistant to sotorasib or adagrasib, suggesting the potential to treat patients who fail therapy with $KRAS^{G12C}$ inhibitors.

ADT-007 exhibits superior growth inhibitory activity compared to RMC-6236 against PDAC cells

Finally, we sought to compare ADT-007 with another pan-RAS inhibitor in clinical trials, RMC-6236. Both $KRAS^{G12D}$ (7160C2, KPC, 2838c3, 6419C5, 5363, HPAC, and HPAC) and $KRAS^{G12C}$ (MIA PaCa-2) mutant PDAC cell lines were treated with ADT-007 or RMC-6236. The results showed that, ADT-007 exhibited significantly improved growth inhibitory activity compared with RMC-6236 across all tested PDAC cells (Supplementary Fig. 9A). This effect was observed in both $KRAS^{G12D}$ and $KRAS^{G12C}$ mutant cells suggesting greater efficacy of ADT-007 in targeting RAS-driven PDAC.

Discussion

PDAC poses a formidable global health challenge as the most lethal cancer with a notable absence of effective treatments [21]. Point mutations in the RAS oncogene family, encompassing KRAS, NRAS, and HRAS are widespread across multiple cancers, but especially mutations in KRAS as a driver of PDAC. Despite the high prevalence of KRAS mutations in the most fatal human cancers, direct targeting of KRAS by reversible inhibitors has been challenging primarily because of the lack of binding surfaces on the protein and high affinity to bind GTP to inhibit GTP activation of effector interactions. The recent FDA approval of covalent $KRAS^{G12C}$ inhibitors for the treatment of non-small cell lung cancer has renewed optimism to study RAS as a druggable target, although currently available $KRAS^{G12C}$ inhibitors have limited use for PDAC given that $KRAS^{G12C}$ mutations are rare in patients diagnosed with PDAC. Recognizing the role of other KRAS mutations in PDAC and other cancers, namely $KRAS^{G12D}$, intensive efforts are ongoing to develop $KRAS^{G12D}$ inhibitors [22].

This present study builds upon our discovery of ADT-007, a reversible, highly potent, and selective pan-RAS inhibitor, with broad growth inhibitory activity and potential to avoid resistance mechanisms limiting the efficacy of mutant or isoform specific RAS inhibitors [14]. As ADT-007 has low water solubility and is rapidly metabolized by glucuronidation, which limits systemic exposure by systemic IV or oral administration, we developed ADT-1004 as an orally bioavailable prodrug of ADT-007. Oral administration of ADT-1004 in mice generated sustained plasma levels of ADT-007 that was amenable to once or twice-daily dosing schedules. In the current study, we selected the 40 mg/kg once daily dose which appeared to be the lowest dose capable of

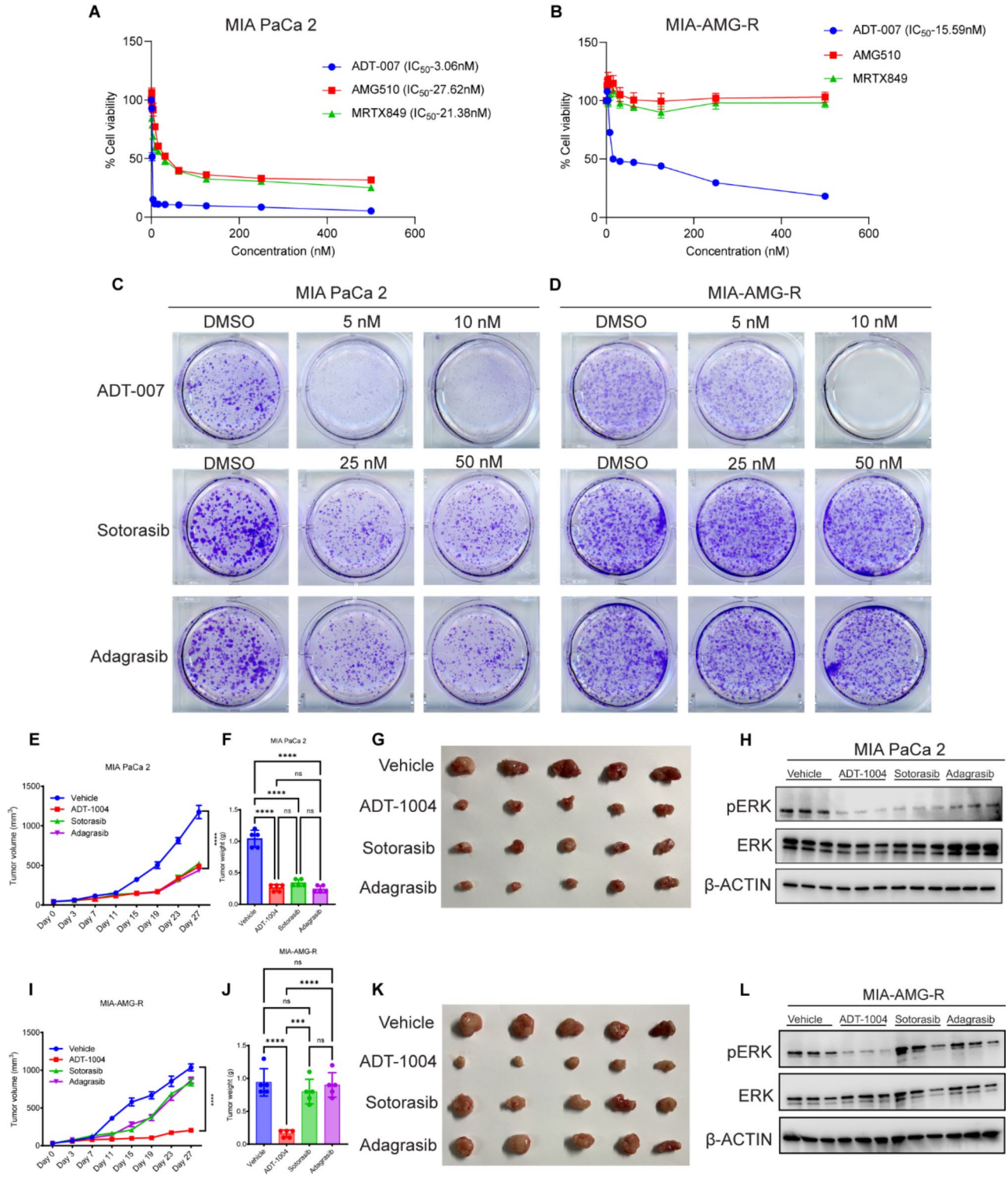

Fig. 7 ADT-1004 demonstrates superior efficacy in suppressing the growth of $KRAS^{G12Ci}$–resistant cells compared to Sotorasib and Adagrasib. (**A-B**). PDAC cell lines were treated with different concentrations of ADT-007, sotorasib, and adagrasib for 3 days and analyzed for survival using the MTT assay. (**C-D**). Indicated PDAC cell lines were treated with the different concentrations of ADT-007, sotorasib or adagrasib for 2 weeks. Representative cell survival was then measured using clonogenic assays. (**E** and **I**). Tumor volumes of mice implanted with MIA PaCa-2 or MIA-AMG-Res cells with the indicated treatments. (**F** and **J**) Tumor weights were measured from mice for the indicated conditions for experiments in (**E** and **I**). (**G** and **K**) Representative tumor images of NSG mice in the vehicle, ADT-1004, Sotorasib, and Adagrasib (40 mg/kg) groups at the end of the experiment. (**H** and **L**). The indicated tumor tissues were probed for pERK and total ERK expression by immunoblotting. β-Actin was used as a loading control. Data represent the mean ± SEM. ANOVA and area under curve (AUC) was used for statistical analysis where appropriate. ns: not significant, $*p < 0.05$, $**p < 0.01$, $***p < 0.001$, and $****p < 0.0001$

achieving plasma levels of ADT-007 exceeding in vitro growth IC_{50} values. Future detailed dose range studies will be needed to better define the ideal dose and schedule of administration of ADT-1004 to optimize anticancer activity in preclinical models.

Antitumor activity of orally administered ADT-1004 against multiple mouse models of PDAC, including orthotopically implanted mouse cell lines and subcutaneously implanted PDX with different KRAS mutations was clearly demonstrated. In addition, orally administered ADT-1004 demonstrated strong inhibitory effects on RAS activation and downstream MAPK signaling by measurement of RAS-GTP and pERK levels, respectively. Previous studies from our group have revealed that treatment of colon and PDAC cell lines with ADT-007 resulted in profound induction of apoptosis and cell cycle arrest at the G2/M phase, further emphasizing its antitumor activity. Furthermore, we have also observed the concurrent inhibition of phospho-cRAF, phospho-MEK, and phospho AKT along with phospho ERK [14]. These findings are also consistent with the published activity of other mutation specific and pan-RAS inhibitors in PDAC [23–25].

Oncogenic KRAS is a significant enabler of the immune suppressive TME in PDAC such that blockage of RAS signaling promotes cytotoxic and M1 pro-inflammatory anti-tumor immune responses [26]. Preclinical studies of mutant specific KRAS inhibitors, demonstrates a critical role of oncogenic KRAS signaling in immune suppression whereby targeting RAS vastly improves tumor immune responses [27]. Our study demonstrates similar immune modulatory potential of ADT-1004 in comparison with other mutation-specific and pan-RAS inhibitors [15, 16, 25]. specifically, treatment with ADT-1004 increases immune infiltration into the 2838c3 TME with increased T cell infiltration. Furthermore, there is an increase in T cells expressing immune suppressive receptors PD-1, CTLA-4, and LAG-3, which are critical for immunosuppression of anti-tumor specific T cell responses [28].

Others have demonstrated that targeted inhibition of oncogenic $KRAS^{G12D}$ signaling with MRTX1133 in preclinical models of PDAC resulted in increases in PD-1, such that blockade of this signaling pathway enhanced antitumor efficacy [15, 29]. Therefore, it is likely that ADT-1004 could enhance efficacy in combination with immune checkpoint inhibitors, although further studies are needed to assess this possibility along with tolerability. The observed increase in macrophage populations indicates a role for ADT-1004 in altering the macrophage phenotype from an immunosuppressive anti-inflammatory (M2-like) to a pro-inflammatory (M1 like) phenotype, which is again consistent with findings using other targeted RAS-inhibitors. Additionally, we observed increases in the abundance of dendritic cell subsets in the 2838c3 TME, which is critical for priming tumor-antigen specific T cells [30]. Interestingly, $CD11b^{+}$ $Ly6G^{+}$ granulocytes in the 2838c3 TME were increased with ADT-1004 treatment. These cells expressed a significant, but modest increase in MHCII and downregulation of PD-L1, suggesting that these cells may exhibit antigen-presentation potential, which has been associated with increased survival in patients with a range of cancers and highlight another novel property of ADT-1004 [31]. Overall, this broad activation of macrophages (and granulocytes) with enhanced T cell priming capabilities suggests the potential of ADT-1004 to enhance antigen presentation and pro-inflammatory responses in the pancreatic TME. We observed a differential immune activation in the KPC model compared to 2838c3. A possible explanations for the observed differences could be related to baseline model-specific differences in the state of myeloid and T cell density and activation demonstrated previously [14]. Another potential contributor to these observed differences may relate to the fact that the KPC cell line exhibits uniform sarcomatoid or mesenchymal morphology in vitro and in vivo as compared to the epithelial morphology observed in 2838c3 [32]. Recent literature suggests that the mesenchymal morphology may influence allele specific RAS inhibitor drug activity and its impact on tumor immunity. EMT phenotype has been reported to be a mechanism of acquired resistance of lung tumors to $KRAS^{G12C}$ inhibitors [33]. Similar observations have been reported by the $KRAS^{G12D}$-specific inhibitor, MRTX1133, in PDAC [34]. Further work is needed to understand the significance of these morphologic variations on sensitivity to pan-RAS inhibitors.

Our spatial analysis of tumor core regions shows cell localization patterns were impacted by ADT-1004 treatment. Of interest, is the enhancement of spatial patterns known in cancer biology as the paucity of infiltration of immune cells around mesenchymal-transitioned cancer cells and FAP^{+} and $Integrin\beta3^{+}$ CAFs. Another desirable feature of ADT-1004 is its cytotoxic ability towards PDAC cells resistant to FDA-approved allele-specific KRAS inhibitors. In this study, we show that human MIA PaCa-2 PDAC cells harboring $KRAS^{G12C}$ developed to be resistant to sotorasib and adagrasib retained sensitivity to ADT-007 in vitro and to ADT-1004 in vivo. Similarly, human AsPC-1 PDAC cells with $KRAS^{G12D}$ developed resistance to MRTX1133 but remained sensitive to ADT-007. Previous clinical studies with $KRAS^{G12C}$ inhibitors have identified multiple mechanisms of intrinsic or acquired resistance. These include new mutations in KRAS or activation of the wild-type KRAS allele or compensation from RAS^{WT} isozymes (e.g., NRAS or HRAS) that are co-expressed with mutant KRAS and activated by growth factors (e.g., EGF) enriched in the TME. These resistance mechanisms can be bypassed by

a pan-RAS inhibitor such as ADT-1004/ADT-007 and provide a key advantage over existing mutant-specific KRAS inhibitors to support clinical development. The ability of ADT-007 to induce mitotic arrest and apoptosis may provide additional advantages to avert resistance as previously reported [14]. For example, ADT-007 completely inhibited colony formation of $KRAS^{G12C}$ PDAC cells, while $KRAS^{G12C}$ inhibitors (sotorasib and adagrasib), KRAS-specific inhibitors (BI-2865) and another pan-RAS inhibitor in development (RMC-6236) were appreciably less effective. Our findings also demonstrate that, ADT-007 exhibited greater growth inhibitory activity than RMC-6236 across multiple PDAC cells with $KRAS^{G12D}$ and $KRAS^{G12C}$ mutations suggesting that ADT-007 might have superior anticancer efficacy by blocking GTP activation of RAS state compared to other inhibitors in development that target RAS in either an off or on conformation.

In conclusion, this study establishes ADT-1004 as a 1st -in-class orally bioavailable pan-RAS inhibitor specific for the apoenzyme state of mutant RAS. ADT-1004 exhibits promising antitumor activity against RAS-mutant PDAC, including resistant phenotypes. The changes in the TME observed with ADT-1004 also suggest that a combination with immune checkpoint inhibitors is a rational approach to evaluate in preclinical models. Future studies to define the optimal dose and schedule of administration of ADT-1004 and establishing a safety in preclinical models will be needed for clinical development of this promising pan-RAS inhibitor.

Limitations of the study

The current study utilized human PDAC cell and PDXs along with murine PDAC models, which are valuable in preclinical research. However, we acknowledge that, these models have limitations in that they may not fully recapitulate the complexity of human PDAC TME or its clonal heterogeneity. While the study used KPC-derived cell lines, future work should include autochthonous mouse models. Given that advanced PDAC can bypass KRAS inhibition through alternative mechanisms, evaluating ADT-1004 in models with metastasis will be needed in future studies. In addition, considering combination therapy with immune checkpoint inhibitors, chemotherapy, or other targeted therapies would be a critical direction to enhance activity against metastatic disease models. Another relevant clinical scenario is the use of ADT-1004 in the neoadjuvant or adjuvant models to suppress or eradicate micro- metastasis. This will also be an important aspect in future studies of ADT-1004.

Supplementary Information

The online version contains supplementary material available at https://doi.org/10.1186/s12943-025-02288-9.

Supplementary Material 1

Supplementary Material 2

Supplementary Material 3

Supplementary Material 4

Supplementary Material 5

Author contributions

Dhana Sekhar Reddy Bandi, Ph.D (Conceptualization: Equal; Investigation: Equal; Methodology: Equal; Validation: Lead; Writing– original draft: Lead; Writing– review &editing: Lead). Dr. Ganji Purnachandra Nagaraju, Ph.D (Conceptualization: Supporting; Formalanalysis: Supporting; Methodology: Supporting; Resources: Lead; Software: Lead; Supervision: Equal; Writing– original draft: Equal; Writing– review & editing: Equal). Sujith Sarvesh, Ph.D (Formal analysis: Supporting; Investigation: Supporting; Methodology: Supporting; Software: Equal; Writing– review & editing: Supporting). Julienne L. Carstens, Ph.D (Software: Equal; Writing– review & editing: Supporting). Jeremy B. Foote, Ph.D (Methodology: Supporting; Validation: Supporting; Writing–review & editing: Supporting). Emily C. Graff, Ph.D (Formal analysis: Supporting). Yu-Hua D Fang, Ph.D (Software: Equal). Adam B. Keeton, Ph.D (Resources: Supporting). Xi Chen, Ph.D (Resources: Supporting). Kristy L. Berry, Ph.D (Resources: Supporting). Sejong L. Bae, Ph.D (Formal analysis: Supporting). Mehmet Akce, MD (Writing– review & editing: Supporting). Greg Gorman, Ph.D (Resources: Supporting). Karina J. Yoon, Ph.D (Resources: Supporting). Upender J. Manne, Ph.D (Resources: Supporting). Micheal R. Boyd, Ph.D (Resources: Supporting). Donald J. Buchsbaum, Ph.D (Writing– review & editing: Supporting). Asfar S. Azmi, Ph.D (Resources: Equal). Yulia Y. Maxuitenko, Ph.D (Conceptualization: Supporting; Formal analysis: Equal; Methodology: Equal; Resources: Equal; Validation: Equal; Writing– original draft: Supporting; Writing– review & editing: Equal). Gary A. Piazza, Ph.D (Conceptualization: Equal; Formal analysis: Supporting; Methodology: Supporting; Project administration: Supporting; Resources: Lead; Supervision: Equal; Writing– original draft: Equal; Writing– review & editing: Equal). Prof. Bassel F. El-Rayes, MD (Conceptualization: Lead; Data curation: Lead; Formalanalysis: Lead; Funding acquisition: Lead; Investigation: Lead; Methodology: Lead; Project administration: Lead; Resources: Lead; Software: Lead; Supervision: Lead; Validation: Lead; Visualization: Lead; Writing– original draft: Lead; Writing– review &editing: Lead). All authors have read and approved the final manuscript and agree to be accountable for all aspects of the work.

Funding

This work was supported by University of Alabama at Birmingham, Birmingham, AL, USA. BE was also supported by Comprehensive cancer center core support grant (5P30CAO13148-47) and 1R01CA294647. GP was supported by NIH/NCI R01CA254197, R01CA238514, and P30CA01314. The authors also acknowledge UAB Flow Cytometry & Single Cell Core Facility grant support Center for AIDS Research (AI027767).

Data availability

No datasets were generated or analysed during the current study.

Declarations

Ethics approval

Not applicable.

Consent to participate

Not applicable.

Consent to publish

Not applicable.

Competing interests

The authors declare no competing interests.

Author details
[1]Department of Hematology and Oncology, O'Neal Comprehensive Cancer Center, Heersink School of Medicine, University of Alabama, Birmingham, AL 35233, USA
[2]Department of Microbiology, University of Alabama, Birmingham, AL 35294, USA
[3]Department of Pathobiology, College of Veterinary Medicine, Auburn University, Auburn, AL 36849, USA
[4]Radiology and Neurology, University of Alabama, Birmingham, AL 35233, USA
[5]Drug Discovery and Development Department, Harrison College of Pharmacy, Auburn University, Auburn, AL 36849, USA
[6]Division of General Internal Medicine and Population Science, University of Alabama School of Medicine, Birmingham, AL 35233, USA
[7]Department of Pharmaceutical, Social and Administrative Sciences, Samford University, Birmingham, AL 35229, USA
[8]Department of Pharmacology and Toxicology, University of Alabama, Birmingham, AL 35233, USA
[9]Department of Pathology, University of Alabama, Birmingham, AL 35233, USA
[10]Department of Obstetrics and Gynecology, University of Alabama, Birmingham, AL 35233, USA
[11]Department of Oncology, Karmanos Cancer Institute, Wayne State University School of Medicine, Detroit, MI 48201, USA
[12]ADT Pharmaceuticals, LLC, Orange Beach, AL 31691, USA
[13]Present address: Department of Cell, Developmental and Integrative Biology, University of Alabama, Birmingham, AL 35294, USA

Received: 21 January 2025 / Accepted: 28 February 2025
Published online: 13 March 2025

References

1. Yousef A, Yousef M, Chowdhury S, Abdilleh K, Knafl M, Edelkamp P, Alfaro-Munoz K, Chacko R, Peterson J, Smaglo BG. Impact of KRAS mutations and co-mutations on clinical outcomes in pancreatic ductal adenocarcinoma. NPJ Precision Oncol. 2024;8(1):27.
2. Mizrahi JD, Surana R, Valle JW, Shroff RT. Pancreatic cancer. Lancet. 2020;395(10242):2008–20.
3. Siegel RL, Miller KD, Wagle NS, Jemal A. Cancer statistics, 2023. Cancer J Clin. 2023;73(1):17–48.
4. Jiang Y, Sohal DP. Pancreatic adenocarcinoma management. JCO Oncol Pract. 2023;19(1):19–32.
5. Siegel RL, Giaquinto AN, Jemal A. Cancer statistics, 2024. Cancer J Clin. 2024;74(1).
6. Bailey P, Chang DK, Nones K, Johns AL, Patch A-M, Gingras M-C, Miller DK, Christ AN, Bruxner TJ, Quinn MC. Genomic analyses identify molecular subtypes of pancreatic cancer. Nature. 2016;531(7592):47–52.
7. McCormick F. KRAS as a therapeutic target. Clin Cancer Res. 2015;21(8):1797–801.
8. Ryan DP, Hong TS, Bardeesy N. Pancreatic adenocarcinoma. N Engl J Med. 2014;371(11):1039–49.
9. Waters AM, Der CJ. KRAS: the critical driver and therapeutic target for pancreatic cancer. Cold Spring Harbor Perspect Med. 2018;8(9):a031435.
10. Ostrem JM, Peters U, Sos ML, Wells JA, Shokat KM. K-Ras (G12C) inhibitors allosterically control GTP affinity and effector interactions. Nature. 2013;503(7477):548–51.
11. Lanman BA, Allen JR, Allen JG, Amegadzie AK, Ashton KS, Booker SK, Chen JJ, Chen N, Frohn MJ, Goodman G. Discovery of a Covalent Inhibitor of KRASG12C (AMG 510) for the Treatment of Solid Tumors. In.: *ACS Publications*; 2019, 52–65.
12. Liu JO. Targeting cancer with molecular glues. Science. 2023;381(6659):729–30.
13. Awad MM, Liu S, Rybkin II, Arbour KC, Dilly J, Zhu VW, Johnson ML, Heist RS, Patil T, Riely GJ. Acquired resistance to KRASG12C inhibition in cancer. N Engl J Med. 2021;384(25):2382–93.
14. Foote JB, Mattox TE, Keeton AB, Chen X, Smith FT, Berry K, Holmes TW, Wang J, Huang C-h, Ward A. A pan-RAS inhibitor with a unique mechanism of action blocks tumor growth and induces antitumor immunity in gastrointestinal cancer. Cancer Res. 2024. https://doi.org/10.1158/0008-5472.CAN-24-0323
15. Canon J, Rex K, Saiki AY, Mohr C, Cooke K, Bagal D, Gaida K, Holt T, Knutson CG, Koppada N. The clinical KRAS (G12C) inhibitor AMG 510 drives anti-tumour immunity. Nature. 2019;575(7781):217–23.
16. Kemp SB, Cheng N, Markosyan N, Sor R, Kim I-K, Hallin J, Shoush J, Quinones L, Brown NV, Bassett JB. Efficacy of a small-molecule inhibitor of KrasG12D in immunocompetent models of pancreatic cancer. Cancer Discov. 2023;13(2):298–311.
17. Li J, Byrne KT, Yan F, Yamazoe T, Chen Z, Baslan T, Richman LP, Lin JH, Sun YH, Rech AJ. Tumor cell-intrinsic factors underlie heterogeneity of immune cell infiltration and response to immunotherapy. Immunity. 2018;49(1):178–93. e177.
18. Carstens JL, Yang S, De Sampaio PC, Zheng X, Barua S, McAndrews KM, Rao A, Burks JK, Rhim AD, Kalluri R. Stabilized epithelial phenotype of cancer cells in primary tumors leads to increased colonization of liver metastasis in pancreatic cancer. Cell Rep. 2021;35(2).
19. Khan HY, Nagasaka M, Aboukameel A, Alkhalili O, Uddin MH, Bannoura SF, Mzannar Y, Azar I, Beal EW, Tobon ME. Anticancer efficacy of KRASG12C inhibitors is potentiated by PAK4 inhibitor KPT9274 in preclinical models of KRAS G12C-mutant pancreatic and lung cancers. Mol Cancer Ther. 2023;22(12):1422–33.
20. Khan HY, Aboukameel A, Uddin MH, Bannoura SF, Keffri K, Jasti M, Virga R, Motorwala S, Choucair K, Hadid T. Next generation nuclear export blocker KPT8602 synergizes with KRASG12D inhibitor MRTX1133 resulting in improved antitumor effects against pancreatic ductal adenocarcinoma. Cancer Res. 2024;84(6Supplement):4574–4574.
21. Neoptolemos JP, Kleeff J, Michl P, Costello E, Greenhalf W, Palmer DH. Therapeutic developments in pancreatic cancer: current and future perspectives. Nat Reviews Gastroenterol Hepatol. 2018;15(6):333–48.
22. Tang D, Kang R. Glimmers of hope for targeting oncogenic KRAS-G12D. Cancer Gene Ther. 2023;30(3):391–3.
23. Hallin J, Bowcut V, Calinisan A, Briere DM, Hargis L, Engstrom LD, Laguer J, Medwid J, Vanderpool D, Lifset E. Anti-tumor efficacy of a potent and selective non-covalent KRASG12D inhibitor. Nat Med. 2022;28(10):2171–82.
24. Wasko UN, Jiang J, Dalton TC, Curiel-Garcia A, Edwards AC, Wang Y, Lee B, Orlen M, Tian S, Stalnecker CA. Tumor-selective activity of RAS-GTP inhibition in pancreatic cancer. Nature. 2024:1–3. https://doi.org/10.1038/s41586-024-07379-z
25. Jiang J, Jiang L, Maldonato BJ, Wang Y, Holderfield M, Aronchik I, Winters IP, Salman Z, Blaj C, Menard M. Translational and therapeutic evaluation of RAS-GTP inhibition by RMC-6236 in RAS-driven cancers. Cancer Discov. 2024;14(6):994–1017.
26. Ischenko I, D'Amico S, Rao M, Li J, Hayman MJ, Powers S, Petrenko O, Reich NC. KRAS drives immune evasion in a genetic model of pancreatic cancer. Nat Commun. 2021;12(1):1482.
27. Molina-Arcas M, Downward J. Exploiting the therapeutic implications of KRAS inhibition on tumor immunity. Cancer Cell. 2024;42(3):338–57.
28. He X, Xu C. Immune checkpoint signaling and cancer immunotherapy. Cell Res. 2020;30(8):660–9.
29. Mahadevan KK, McAndrews KM, LeBleu VS, Yang S, Lyu H, Li B, Sockwell AM, Kirtley ML, Morse SJ, Diaz BAM. KRASG12D inhibition reprograms the microenvironment of early and advanced pancreatic cancer to promote FAS-mediated killing by CD8+T cells. Cancer Cell. 2023;41(9):1606–20. e1608.
30. Gardner A, de Mingo Pulido Á, Ruffell B. Dendritic cells and their role in immunotherapy. Front Immunol. 2020;11:924.
31. Wu Y, Ma J, Yang X, Nan F, Zhang T, Ji S, Rao D, Feng H, Gao K, Gu X. Neutrophil profiling illuminates anti-tumor antigen-presenting potency. Cell. 2024;187(6):1422–39. e1424.
32. Guo CC, Majewski T, Zhang L, Yao H, Bondaruk J, Wang Y, Zhang S, Wang Z, Lee JG, Lee S. Dysregulation of EMT drives the progression to clinically aggressive sarcomatoid bladder cancer. Cell Rep. 2019;27(6):1781–93. e1784.
33. Adachi Y, Ito K, Hayashi Y, Kimura R, Tan TZ, Yamaguchi R, Ebi H. Epithelial-to-mesenchymal transition is a cause of both intrinsic and acquired resistance to KRAS G12C inhibitor in KRAS G12C–mutant non–small cell lung cancer. Clin Cancer Res. 2020;26(22):5962–73.

34. Gulay KCM, Zhang X, Pantazopoulou V, Patel J, Esparza E, Pran Babu DS, Ogawa S, Weitz J, Ng I, Mose ES. Dual inhibition of KRASG12D and pan-ERBB is synergistic in pancreatic ductal adenocarcinoma. Cancer Res. 2023;83(18):3001–12.

Publisher's note